Journal of Power Sources, 32 (1990) 277 - 286

ELECTROCHEMICAL BEHAVIOUR OF IRON OXIDE ELECTRODES IN ALKALI SOLUTIONS

N. JAYALAKSHMI and V. S. MURALIDHARAN*

Central Electrochemical Research Institute, Karaikudi 6 (India)

(Received August 4, 1989; in revised form April 2, 1990)

Summary

The need for understanding the electrochemical behaviour of iron oxide in iron electrodes arises mainly due to development of iron electrodes for alkaline batteries. The charge and discharge behaviours of pressed and sintered iron oxide electrodes in electrolytic iron powder were studied by triangular potential sweep voltammetry, chronopotentiometry open circuit potential decay and recovery transient techniques. The role of oxide in the iron electrode for the nickel–iron cell is discussed.

Introduction

The improvement in iron electrode performance is of practical significance because of its use in alkaline accumulators. The performance can be improved either by mixing additives with the iron powder before sintering or by dissolution in the electrolyte [1 - 8]. An earlier reference reports how magnetite was mixed in a copper electrode which was then subsequently reduced with 90% efficiency in strong alkali. Unfortunately the capacity was found to be limited on discharge [9]. The behaviour of iron oxide electrodes in the presence of various dopants has already been reported [10]. The present study deals with the electrochemical behaviour of α-Fe_3O_4 added to the electrolytic iron powder in various amounts before forming, either by pressing or sintering methods.

Experimental

Preparation of iron oxide electrodes

Sintered electrodes

The electrolytic iron powder (α-Fe) has the composition (99.1wt.%Fe–0.01wt.%Pb–0.008wt.%Zn–0.001wt.%As–0.025wt.%Mn–0.005wt.%Cu) and

*Author to whom correspondence should be addressed.

0378-7753/90/$3.50

300 mesh particle size; loose sintered electrodes were prepared from iron powder and the mixture of iron oxide and iron. The powders were spread uniformly over a 10 mesh nickel grid of 0.1 mm thickness and area 1.67 cm^2. The electrodes were sintered at 1173 K for 1 h in a hydrogen atmosphere. Copper rod was welded to the pellet to provide electrical connections. The number of Fe^{2+} ions in α-Fe_3O_4 was estimated by the usual methods [11].

Pressed electrodes

The electrodes were prepared by pressing the electrode mix to 3 to 5 PSI in the form of a pellet of 10 mm diam. and 3 mm thickness. The electrode mix contained electrolytic iron powder with varying amounts of α-Fe_3O_4. For electrochemical studies these pellets were pressed into a Teflon socket and electrical connections were made. Table 1 presents the details of the electrodes prepared and their respective composition.

Electrochemical studies

Triangular potential sweep voltammetry (TPSV)

The system consisted of a voltage scan generator (Wenking model VSG 72), potentiostat (Wenking 70 TSI), X-Y-t recorder and a digital multimeter. Pressed iron oxide electrodes were used in a three electrode cell assembly.

Chronopotentiometry

The cell employed a sintered iron oxide electrode as the working electrode, platinum foil as the auxillary electrode and Hg/HgO as the reference electrode. The oxide electrodes were cathodically polarised using a constant current source for 1 h applying various currents (300 to 1000 mA) depending on the Fe_3O_4 content. At the end of 1 h, different anodic current steps in the range 15 - 45 mA were applied. The potential was then followed for 1 h using a printing voltmeter. Before applying the next anodic current step, the electrode was made cathodic for a period of 1 h.

TABLE 1

Composition of sintered and pressed iron oxide electrodes

Type	Electrode	Composition (%)		
		Fe	Fe^{2+}	Fe^{3+}
Sintered	A	99.1		
	B	64	22	3
	C	50	31	18
	D	35	41	23
Pressed	E	99.1		
	F	78	12	9
	G	69	16	12
	H	64	22	3

Open circuit potential transient studies

The sintered oxide electrodes were cathodically polarised at different currents for 1 h. The current values were 300 - 1000 mA depending on the α-Fe_3O_4 content. The currents were switched off at the end of 1 h and the open circuit potential decay was followed with time. The steady values were noted.

Open circuit potential recovery studies were made at the end of anodic polarisation by breaking the circuit. The open circuit potential *versus* time was followed using a printing voltmeter.

Experiments were carried out in 6 M KOH with 0.63 M LiOH at 30 ± 0.01 °C. The solutions were prepared with analar chemicals using double distilled water. The potentials were measured using Hg/HgO electrodes and no corrections were made for liquid junction potentials.

Results

TPSV studies

A pressed iron electrode was kept at −1.3 V for 5 min, disconnected, shaken free of attached hydrogen bubbles and polarised to −0.5 V. In 6.0 M solutions, the electrochemical spectrum (Fig. 1) revealed in the forward (v = 10 mV s^{-1}) scan peak I at −840 mV, peak II at −630 mV and, in reverse, peak III at −970 mV followed by a small peak IV at −1130 mV on subsequent sweeping. The charges under the peaks increased suggesting that the reactions are sequential and superimposed. The zero crossing potential (*ZCP*) in the forward scan occurred at −1040 mV while in the reverse scan it occurred at −800 mV. In the forward scan the appearance of peak I is due to the conversion of Fe to $Fe(OH)_2$ followed by further oxidation to FeOOH at −630 mV. The *ZCP* at −800 mV in the reverse scan arises due to incomplete reduction of the oxide on the surface. The appearance of peaks III and IV is due to the reduction of FeOOH to $Fe(OH)_2$ or $HFeO_2^-$ followed by ultimate reduction back to Fe. This is similar to those reported earlier [3].

Figure 2 presents the electrochemical spectrum obtained from a pressed iron electrode containing 30% Fe_3O_4. In the forward scan *ZCP* occurred at −1040 mV followed by a single anodic peak at −870 mV. The reverse scan exhibited a single cathodic peak at −1040 mV followed by hydrogen evolution above −1200 mV. For 30% Fe_3O_4, the cathodic peak disappeared at sweep rates above 1 mV s^{-1}. The appearance of an anodic peak rather than a plateau is due to the kinetic hindrance of the subsequent oxidation step of $Fe(OH)_2$ to FeOOH. The reduction process $Fe(OH)_2$ to Fe is completely reversible, however. The oxidation of $Fe(OH)_2$ to FeOOH does not appear to take place in the potential range studied.

When the Fe_3O_4 content was raised to 40% the anodic peak appeared at −840 mV while the reduction peak appeared at −1000 mV. For the sweep rate range of 0.1 - 10 mV s^{-1} the cathodic peak potential is independent of v. In the forward scan beyond −600 mV, the oxidation of $Fe(OH)_2$ to FeOOH was found to take place (Fig. 3).

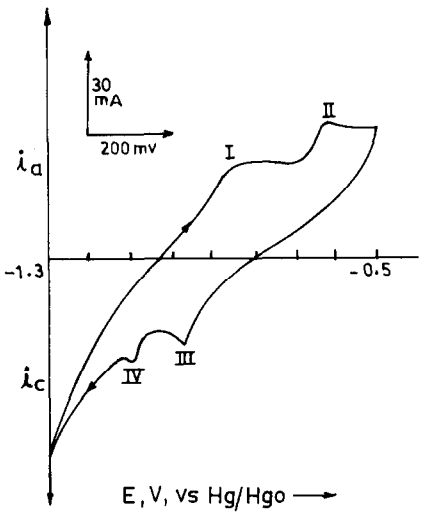

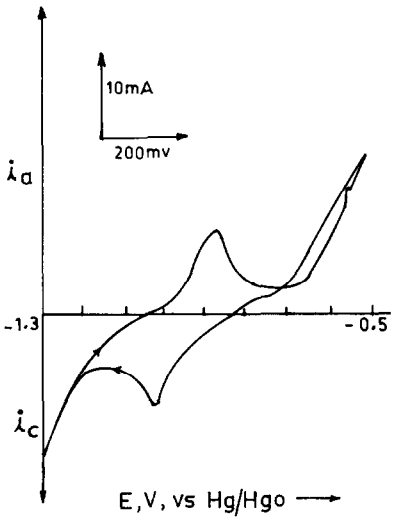

Fig. 1. Typical cyclic voltammogram for pressed iron electrode in 6.0 M KOH and 0.63 M LiOH solution. Sweep rate = 10 mV s^{-1}; $E_{\lambda,c} = -1.3$ V, $E_{\lambda,a} = -0.5$ V.

Fig. 2. Typical cyclic voltammogram for pressed iron + 30% iron oxide in 6.0 M KOH and 0.63 M LiOH solution. Sweep rate = 0.5 mV s^{-1}; $E_{\lambda,c} = -1.3$ V; $E_{\lambda,a} = -0.5$ V.

Further increase of Fe_3O_4 to 50% resulted in the complete disappearance of the cathodic peak and hydrogen evolution was found to occur above −1100 mV. The appearance of a single broad anodic peak (Fig. 4) at −800 mV is due to complete conversion of Fe to $Fe(OH)_2$ and *ZCP* was found to take place at −630 mV during the reverse scan.

Chronopotentiometric studies

An assumption is made that all the applied anodic currents favour the reaction between the electrode and hydroxyl ions and that mass transfer is

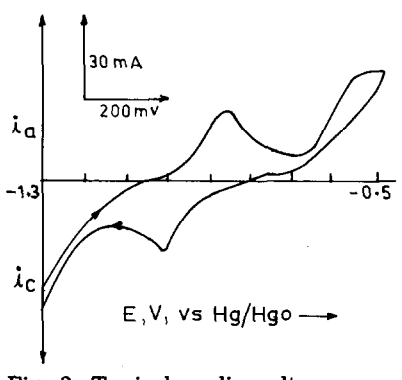

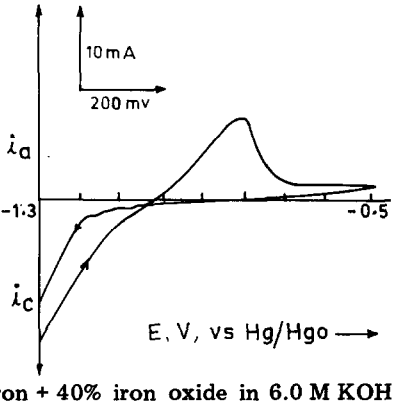

Fig. 3. Typical cyclic voltammogram for pressed iron + 40% iron oxide in 6.0 M KOH and 0.63 M LiOH solution. Sweep rate = 0.5 mV s^{-1}; $E_{\lambda,c} = -1.3$ V, $E_{\lambda,a} = -0.5$ V.

Fig. 4. Typical cyclic voltammogram for pressed iron + 50% iron oxide in 6.0 M KOH and 0.63 M LiOH solution. Sweep rate = 0.5 mV s^{-1}; $E_{\lambda,c} = -1.3$ V; $E_{\lambda,a} = -0.5$ V.

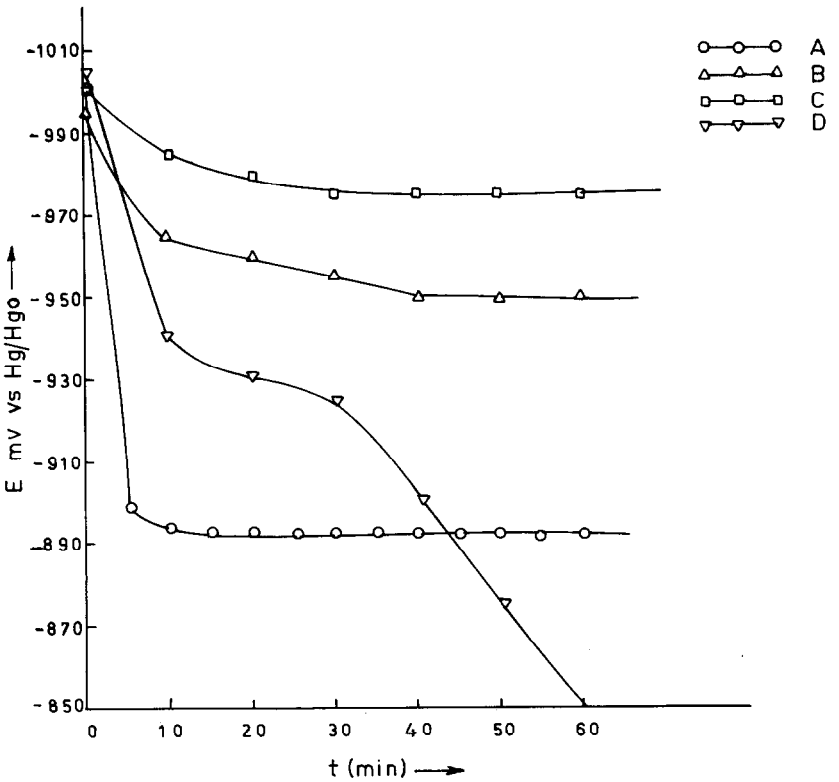

Fig. 5. Typical chronopotentiogram obtained for iron oxide electrodes at an applied anodic current of 20 mA.

controlled by the diffusion of the OH^- ion. Figure 5 presents a typical chronopotentiogram obtained for sintered iron oxide electrodes at 20 mA applied current. The fall in potential is sharp for the iron electrode whereas it is sluggish in the case of the oxides. In the case of 90% iron oxide electrodes the constant potential region or plateau is not observed except at the lower current of 15 mA. A near constant potential region with time (τ) is due to the oxidation of adsorbed hydrogen and conversion of Fe to $Fe(OH)_2$ with thickening of the oxide film. Table 2 presents the parameters derived from these curves. It may be seen that the plateau potentials lie in between the equilibrium potentials of $Fe/Fe(OH)_2$ and $Fe(OH)_2/FeOOH$. With increasing Fe_3O_4 content the plateau potentials become more active suggesting that the oxidation of $Fe/Fe(OH)_2$ is favoured while increasing anodic current shifted the potential towards more noble values. Transition time (τ) decreased with increase in oxide content.

To use these sintered electrodes as negative electrodes in Ni/Fe alkaline batteries, the percentage utilisation of the active material at different applied currents is given in Table 3.

TABLE 2

Parameters derived from chronopotentiograms

Electrode	Current applied					
	15 mA		20 mA		30 mA	
	E (mV)	τ (min)	E (mV)	τ (min)	E (mV)	τ (min)
A	−930	55	−892	45	−875	45
B	−955	50	−950	40	925	40
C	−978	40	−975	40	−940	40
D	−982	20				

TABLE 3

Percentage utilisation of the active material

Current passed (mA)	15	20	30
$Q_{applied} \times 10^3$ (A h)	15	20	30
$Q_{consumed} \times 10^3$ (A h) (% utilisation)			
Electrode A	13.75 (91.6)	15 (75)	22.5 (75)
Electrode B	12.5 (83.3)	13.3 (66.7)	20 (66.7)
Electrode C	10 (66.7)	13.3 (66.7)	20 (66.7)
Electrode D	5 (33.3)		

$$\% \text{ utilisation} = \frac{Q_{consumed}}{Q_{applied}}$$

With increasing oxide content and applied current the percentage utilisation decreases. This may be due to the increase in Fe(III) content and decrease of the active content namely Fe.

A plot of E_c (plateau potential) *versus* applied current yields a slope of 110 ± 10 mV (Fig. 6). This suggests that increasing the oxide content has not affected the mechanism of formation of $Fe(OH)_2$.

Open circuit potential (OCP) transient studies

The oxide electrodes were polarised in the current range of 300 - 1000 mA for electrodes A - D. The OCP decay transients obtained for 30 min (Fig. 7) revealed that the steady potentials lie above the reversible potentials of $Fe(OH)_2/Fe$ and H_2O/OH^-. This suggests that with increasing oxide content the electrodes tried to behave like a hydrogen electrode.

Table 4 presents the corrosion potentials obtained from OCP recovery transients after different anodic polarisation conditions. It may be seen that with increasing oxide content, the potentials shifted in an active direction for 15 mA and that an increase of the anodic current shifted the potential to more negative values. This suggests that the formation of $Fe/Fe(OH)_2$ is favoured by an increase in the oxide content.

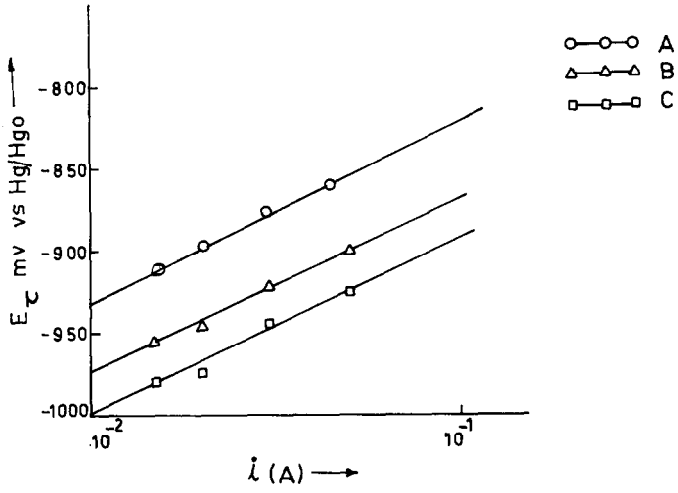

Fig. 6. E_τ *vs.* log *i* plot obtained from chronopotentiograms.

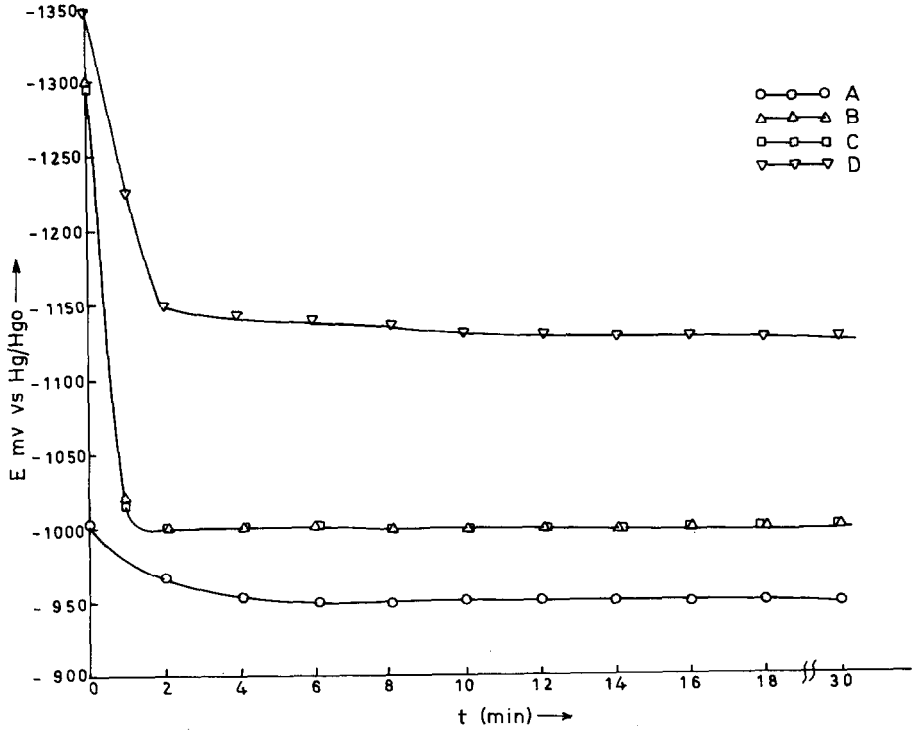

Fig. 7. Open circuit potential decay transitients for iron oxide electrodes.

TABLE 4

Variation of corrosion potential (mV *vs.* Hg/HgO) with increase in Fe_3O_4 at different anodic currents

Electrode	Anodic current (mA)			
	15	20	30	45
A	−980	−981	−984	−990
B	−998	−999		−940
C	−1000	−1006	−1003	−1002
D	−1008	−1008	−974	

Discussion

X-ray, electron diffraction, *in situ* IR spectroscopy and electrochemical methods have identified the anodic films formed on iron as $Fe(OH)_2$, Fe_3O_4, Fe_2O_3 and $Fe_2O_3 \cdot H_2O$ under varying conditions [12 - 16]. Discharge products on iron electrodes revealed the formation of $Fe(OH)_2$ during the first level and Fe_3O_4 and FeOOH at the end of the second level [17, 18]. The plot of E_t *versus* log i revealed a slope of 110 ± 10 mV and suggests

$$Fe + OH^- \longrightarrow (FeOH)_{ads} + e^-$$

$$(FeOH)_{ads} \rightleftharpoons FeOH^+_{ads} + e^-$$

$$Fe(OH)^+_{ads} + OH^- \rightleftharpoons Fe(OH)_2$$

The formation of higher valent oxide films is closely related to the growth of oxide films in air. Sato and Cohen [19] proposed a place exchange mechanism for oxide growth in neutral solutions. The film growth proceeds by the field assisted place exchange of metal oxide pairs. For carbon steel in concentrated NaOH solutions, the dependence of E_p and i_p on v suggested the possible low field migration of ions through an oxide/hydroxide as a slow step [20, 21]

$$i = \left(\frac{nFK}{V_m}\right)v$$

where V_m is the molar volume of the film. Over the $Fe(OH)_2$ surface the oxidation may proceed as

$$OH^-_{solution} \rightleftharpoons OH^-_{oxide}$$

$$OH^-_{oxide} \longrightarrow O^{2-}_{lattice} + H^+_{solution}$$

The incorporation of O^{2-} into the lattice is claimed to be rate controlling. An analysis of $E_{p,a}$ for oxide electrodes containing varying amounts of Fe_3O_4 (Fig. 8) revealed a linear relationship passing through the origin. This suggests that oxidation proceeds via low field migration of ions through an oxide/solution interface.

Increase of oxide content shifted the anodic peak potential to more noble values enhancing the overvoltage for the formation of $Fe(OH)_2$. This may be due to decrease in iron content and the increase of FeO in the mixture. The appearance of the cathodic peaks at about −1140 mV (Figs. 2 and 3) is likely to be due to the reduction of FeOOH to $Fe(OH)_2$. The conversion of $Fe(OH)_2$ to Fe may be convoluted with the hydrogen evolution process. This would explain why the data in Fig. 4 show neither an anodic peak due to FeOOH formation nor an associated reduction peak.

The implication is that the presence of Fe_3O_4 slows the process of conversion of $Fe(OH)_2$ to FeOOH. The reason for this retardation phenomenon could be because the Fe_3O_4 is in redox equilibrium with the newly formed $Fe(OH)_2$ as

$$Fe_3O_4 + 2H^+ + 2e^- \rightleftharpoons Fe(OH)_2 + 2FeO$$

This $Fe(OH)_2$ may undergo reduction to Fe via $(FeOH^+)_{ads}$. The cathodic peak potential shifted from −1040 to −1000 mV when the oxide content was increased by 10%. Further increase of the oxide content causes the disappearance of the cathodic peak. This disappearance in the case of 50% oxide may be due to (i) the modification of the surface or (ii) the iron formed by the reduction of oxides may have low hydrogen over voltage compared to that of electrolytic iron powder used. Hydrogen evolution takes place along with the reduction of oxides.

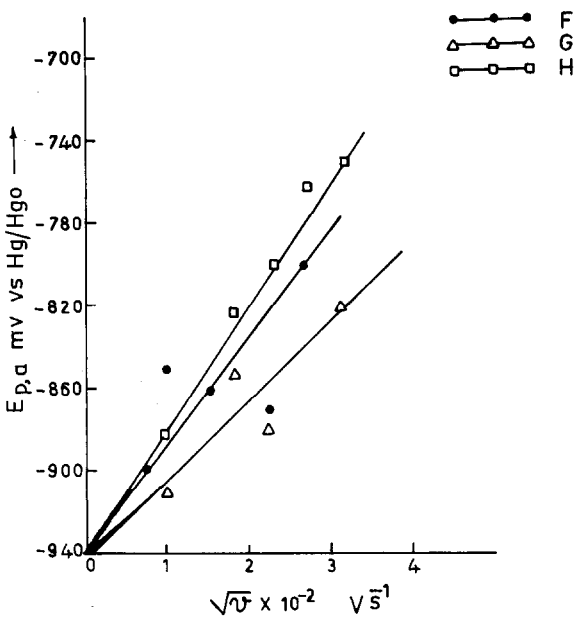

Fig. 8. Anodic peak potential decay *vs.* sweep rate plot obtained for oxide electrodes.

Conclusions

Studies on the oxide electrodes revealed the first electron transfer as a slow step for the formation of $Fe(OH)_2$ on iron. On anodic polarisation further growth of oxide proceeds via low field migration of ferrous ions. Increase of the Fe_3O_4 content slows the conversion of $Fe(OH)_2$ to FeOOH. Hydrogen evolution takes place along with oxide reduction in the presence of oxide.

List of symbols

$E_{\lambda,a}$	Anodic terminal potential
$E_{\lambda,c}$	Cathodic terminal potential
F	Faraday
V_m	Molar volume of the film
n	Number of electrons
i_p	Peak current
E_p	Peak potential
E	Plateau potential
v	Sweep rate
τ	Transition time
ZCP	Zero crossing potential

References

1 L. Ojefors, *Electrochim. Acta, 21* (1976) 302.
2 P. R. Vassie and A. C. C. Tseung, *Electrochim. Acta, 21* (1976) 263.
3 G. Paruthimal Kalaignan, V. S. Muralidharan and K. I. Vasu, *J. Appl. Electrochem., 17* (1987) 1083.
4 G. Paruthimal Kalaignan, V. S. Muralidharan and K. I. Vasu, *Trans. SAEST, 22* (1987) 67.
5 G. Paruthimal Kalaignan, V. S. Muralidharan and K. I. Vasu, *Bull. Electrochem., 4* (1988) 551.
6 G. Paruthimal Kalaignan, V. S. Muralidharan and K. I. Vasu, *Proc. Ann. Tech. Meet. Electrochemical Society of India, Bangalore, July 1985,* Oriel Press, Newcastle upon Tyne, U.K., p. 32.
7 J. Corney and K. Micks, *J. Power Sources, 25* (1989) 111.
8 N. Jayalakshmi and V. S. Muralidharan, *B. Corr. J.*, in press.
9 J. Labat, J. C. Jarrousseau and J. F. Laurent, *Power Sources 3,* 1971, p. 283.
10 K. Micka and Z. Zabransky, *J. Power Sources, 19* (1987) 315.
11 I. Vogel, *Textbook of Quantitative Inorganic Analysis,* Longman, London, 4th edn., 1978, p. 354.
12 H. G. Silver and E. Leaks, *J. Electrochem. Soc., 117* (1970) 5.
13 L. Ojefors, *J. Electrochem. Soc., 123* (1976) 169.
14 A. M. Pritchand and B. J. Mould, *Corros. Sci., 11* (1971) 1.
15 EY. Geronov, I. Tomov and S. Georgier, *J. Appl. Electrochem., 5* (1975) 351.
16 H. Neugebauer, W. Tschinkel, G. Nauer and A. Neckel, *Ext. Abstr., ISE 38th Meet., 1987,* Vol. 1, p. 372.
17 T. K. Teplinskaya, N. N. Feoorova and S. A. Rozentsveig, *Zh. Fiz. Khim, 38* (1964) 2176.
18 A. J. Salkind, C. J. Venuto and S. U. Falk, *J. Electrochem. Soc., 111* (1964) 493.
19 N. Sato and M. Cohen, *J. Electrochem. Soc., 111* (1964) 512, 519.
20 D. E. Williams and G. A. Wright, *Electrochim. Acta, 21* (1976) 1009.
21 D. D. Macdonald and B. Roberts, *Electrochim. Acta, 23* (1978) 781.